Disordered but primitive gallosilicate hydro-sodalite: structure and thermal behaviour of a framework with novel cation distribution

Lars Robben [a], Marius Wolpmann [a], Patrick Bottke [b], Hilke Petersen [a], Malik Šehović [a], Thorsten M. Gesing [a]

a) University of Bremen, Institute for Inorganic Chemistry and Crystallography, Leobener Str. 7, 28359 Bremen, Germany and MAPEX Center for Materials and Processes, Bibliotheksstr. 1, 28359 Bremen, Germany

b) University of Oldenburg, Institute for Technical Chemistry, Carl-von-Ossietzky Str. 9-11, 26129 Oldenburg, Germany

Abstract:

The structure of a new gallosilicate sodalite $|Na_{6.16(1)}(H_2O)_8|[Ga_{1.04(1)}Si_{0.96(1)}O_4]_6$ described in space group $P\bar{4}3n$ with lattice parameter a = 885.208(7) pm is reported. For such a sodalite with a deviation from a 1:1 ratio in the framework cations a body-centred structure in space group $I\bar{4}3m$ could be expected. The structure shows structural stress resulting from this unusual substitution by a high strain visible in reflections which are forbidden by symmetry in $I\bar{4}3m$. Distinct amounts of Ga and Si are redistributed on the opposite crystallographic position. The second coordination sphere of Si was examined by ^{29}Si MAS NMR, the absence of OH^- in the sodalites cages was checked by FTIR- and Raman spectroscopy. The intensity distribution of MAS NMR signal is modelled using a new technique to calculate the framework metal second neighbour coordination. The confirmed distribution leads to a low thermal stability of the cubic sodalite indicated by a new intermediated phase which could be regarded as a triclinic distorted cancrinite with three-time increased *c* lattice parameter. This intermediate phase decomposes at around 1000 K to a beryllonite-type sodium gallosilicate.

Keywords: Sodalite; MAS-NMR spectroscopy; Temperature-dependent behaviour

1. Introduction

Sodalites are a well-known group of zeolitic materials, consisting of a framework of corner sharing MO_4 tetrahedra, building the so-called *sod*-cages. These *sod*-cages contain extra-framework cations (in most cases Na^+), necessary for charge compensation, anions and/or water. Fischer and Baur [1] gave a comprehensive overview on observed sodalite structures and their chemical composition. An alternative structural description via different stacking patterns of sheets of not connected $(M^1M^2O_4)_3$ six-ring sheets leads either to cancrinite (…AB… stacking in <001> direction), sodalite (…ABC… stacking in <111> direction) [2] or the so called intermediate phase with a distinct stacking disorder [3,4]. Generally, the resulting structures could be described in the cancrinite case in hexagonal space-groups (often $P6_3$) with lattice parameter *a* around 1260 pm and *c* around 520 pm in the aluminosilicate system (e.g. [5]), slightly larger ones are observed in the gallosilicate system ($a \approx 1278$ pm, $c \approx 528$ pm [6]). The second stacking sequence, leading to sodalite structures, is predominantly described in cubic space groups, where the most prominent one is $P\bar{4}3n$ [1].

In the compound described here Ga^{3+} and Si^{4+} form the framework, Na^+ and H_2O are the cage filling constituents. Such gallosilicate hydro-sodalites and their synthesis have been described first by Suzuki and co-workers [7] reporting no structural data but a lattice parameter of 885.6 pm. The gallosilicate hydro-sodalites reported by McCusker et al. [8] ($P\bar{4}3n$, Si/Ga = 1.26, a = 885.62(1) pm) and Newsam and Jorgensen [9] ($P\bar{4}3n$, Si/Ga = 1.252, a = 884.75(1) pm) are no pure hydro-sodalites but basic/hydro-sodalites, containing a distinct amount of OH^- groups in their cages. In both cases the Si/Ga ratio is greater than 1. Nenoff et al. (1994) [10] reported a pure gallosilicate hydro-sodalite ($P\bar{4}3n$, Si/Ga = 1, a = 886.14(2) pm) and excluded the presence of OH^- groups. Gesing [11] synthesized a primitive ($P\bar{4}3n$, Si/Ga = 1, a = 885.92(3) pm) and a body-centred ($I\bar{4}3m$, Si/Ga = 1.5, a = 884.148(4) pm) gallosilicate hydro-sodalite. In the latter work the local Si environment

was examined by ^{29}Si MAS-NMR, showing in the first case a single signal with a chemical shift of -75.6 ppm and in the latter one five signals in the chemical shift range of -75.5 ppm to -100.8 ppm corresponding to a local $Si(O_4Ga_4)$, $Si(O_4Ga_3Si)$, $Si(O_4Ga_2Si_2)$, $Si(O_4GaSi_3)$ and $Si(O_4Si_4)$ environment, respectively. The presence of OH^- ions was excluded by vibrational spectroscopy.

From a structural point of view a cubic sodalite with a statistical occupancy on the framework tetrahedral site ($M^1/M^2 \neq 1$, with M^1 and M^2 carrying different charges) should crystallize in space group $I\bar{4}3m$, with the M atoms on a ***12d*** site. A M^1/M^2 ratio of 1 generally means an ordered distribution of the two species and thus leads from the aristotype $Im\bar{3}m$ via the fully expanded structure in $Pm\bar{3}n$ to the partially collapsed structure described in space group $P\bar{4}3n$ with the M^1 and M^2 atoms on the ***6c*** and ***6d*** sites, respectively. Substitution on one of these M sites with an equally charged species retains the space-group [12], substitution with differently charged species inevitably leads to a charge compensating substitution on the other M site, leading to a reduction of symmetry to space group $I\bar{4}3m$.

The dehydration and thermal decomposition of aluminosilicate hydro-sodalites and basic/hydro-sodalites have been examined by Felsche and Luger [9]. They observed the dehydration of several $\left|Na_{6+x}(OH)_x(H_2O)_n\right|[AlSiO_4]_6$ compounds and observed that the compounds with x = 2, n = 4 and x = 0, n = 8 show a dehydration to one resulting phase. The compound with x = 1 and n = 4 shows a splitting (or bifurcation) of the (110) and (211) reflections, which was interpreted as the dehydration to a two-phase mixture of an empty sodalite (x, n = 0) and a basic sodalite ($x \neq 0$, n = 0). The dehydration and decomposition of $\left|Na_6(H_2O)_8\right|[GaSiO_4]_6$ was examined by Gesing [11] and it was shown that the sodalite shows only amorphous humps in the X-ray diffraction pattern between 823 K and 923 K and at higher temperatures the crystallization of a hexagonal beryllonite-type $NaGaSiO_4$ ($P6_3$, with lattice parameters a = 881.5(12) pm and c = 845.6(10) pm at 1073 K). Between 323 K

and 523 K the gallosilicate hydro-sodalite expands from 886.0(4) pm to 890.1(8) pm, which gives an average linear thermal expansion coefficient of $\bar{\alpha}_{a\,323}^{523}$ = 23(1) 10^{-6} K^{-1}, with respect to the lattice parameter *a*.

This study presents the results of in-depth structural examinations of a gallosilicate hydro-sodalite with an unusual distribution of the framework atoms and its thermal stability.

2. Experimental

$NaGaO_2$ was synthesized by mixing dry Na_2CO_3 with Ga_2O_3 in a 1:1 ratio and heating it for 24 h at 1123 K in a corundum crucible. A possible incorporation of Al from the crucible in the $NaGaO_2$ could not be observed (see supporting information). 10 mmol $NaGaO_2$ and Na_2SiO_3 were separately stirred for 10 min with 12.5 mL deionized H_2O to form gels. These gels were mixed with 2 g Na_2CO_3, filled in polytetrafluoroethylene-coated steel autoclaves and heated in an open furnace at 453 K for 41 h.

Temperature-dependent (TD) powder X-ray diffraction data were collected between 300 K and 1300 K in 20 K steps on a Philips X'Pert Pro diffractometer (Panalytical, Almelo, Netherlands), using a HTK1200N high-temperature chamber (Anton Paar, Graz, Austria) and $CuK\alpha_{1,2}$ radiation. The instrument was equipped with a Ni-Filter and an X'Celerator detector system. Rietveld refinements were carried using "DiffracPlus Topas 4.2" (Bruker AXS GmbH, Karlsruhe, Germany) software and the fundamental parameter approach on the refinements. The fundamental parameter set was obtained by fitting instrumental parameters against a LaB_6 standard reference material and has been verified by Si standard reference material. Further details of the refinements are given in the Results and discussion section. An autocorrelation analysis of the TD X-ray data was carried out according to the procedure given in [15].

FTIR data in the spectral range from 370 cm^{-1} to 5000 cm^{-1} were collected on a Bruker Optics IFS 66v spectrometer, measuring 64 scans with a spectral resolution of 2 cm^{-1}. The samples were prepared by the KBr-pellet method: A finely ground mixture of 2 mg sample with 200 mg of KBr was compacted in a closed die for 7 minutes using a pressure of 10^5 N. Raman spectra were collected on a Horiba LabRAM Aramis spectrometer utilizing an Olympus BX-41 confocal microscope and a laser exiting a wavelength of $\lambda = 633$ nm. The sample was slightly pressed to get a smooth and flat sample surface.

Simultaneous thermogravimetric and dynamic difference calorimetry measurements were carried out using a Mettler Toledo TGA/DSC 3+ system. 9.962(1) mg of sample was measured in a corundum crucible in the temperature range of 303 K to 1373 K. A heating rate of 10 K/min, a cooling rate of 20 K/min and an N_2 atmosphere as protective gas with a flow-rate of 20 mL/min was utilized.

^{29}Si MAS NMR spectra were recorded using a Bruker 500 WB spectrometer operating at 11.7 T; the corresponding Larmor frequency was 99.4 MHz, the rotating frequency 15 kHz and a standard 4.0 mm probe head (Bruker WVT-type) was employed. The 1D spectrum was recorded with a single pulse sequence accumulating 400 scans with a delay of 10 minutes. The pulse length was 4 µs at a power level of 200 W. $Si(SiMe_3)_4$ served as secondary reference to determine the chemical shifts. The controlled temperature of the bearing gas (300.0 K) and calibration curve with the reference material leads to an estimated sample temperature of 338(2) K. The long relaxation delay guarantees full longitudinal relaxation of all spectral components and was optimized by a classical saturation recovery experiment.

3. Results and discussion

3.1. Structure at ambient condition

One important question when synthesizing sodalites is the incorporation of water and/or OH-groups. The sodium content depends on one hand on the framework charge and on the other hand on the template charge. FTIR- and Raman-spectra (Figure 1) of the title-compound both show distinct features in the range of the H-O-H bending and the OH^- stretching vibrations. The spectral range of the OH^- stretching vibrations (3000 cm^{-1} - 4000 cm^{-1}) indicates three distinct bands, which can also be observed in the water bending range of the FTIR spectrum (1600 cm^{-1} - 1800 cm^{-1}). The same spectral ranges in the Raman-spectrum shows only two bands, the vibrational mode with the highest Raman shift could not be observed due to its low intensity. The vibrational spectroscopy results do not indicate any incorporation of OH^- into the structure, all stretching vibrations show corresponding bending vibrations.

The average structure was determined using the powder pattern collected at 300 K out of the TD X-ray powder diffraction data set (**Figure *2***). The initial refinements in space group $P\bar{4}3n$ gave no satisfying results with respect to the calculated intensities and peak shapes (R_{wp} = 16.9%). They lead to a high isotropic displacement parameter of the framework oxygen and negative isotropic displacement parameter of the water oxygen atom. A refinement in space group $I\bar{4}3m$ and a mixed occupancy of Si and Ga on the ***12d*** site explained the observed intensities better (R_{wp} = 15.6%), but could not explain several reflections, which are observed but in the body-centred space group forbidden by symmetry. Additionally, these refinements lead to an implausible high isotropic displacement parameter of the framework oxygen atom and to a Si/Ga ratio of 3. A refinement in space group $P\bar{4}3n$ with a mixed occupancy of Si and Ga on the ***6c*** and ***6d*** sites constrained to unity can explain all observed reflections and intensities. Nevertheless, they could not fit well the peak shapes of the reflections symmetry forbidden in space group $I\bar{4}3m$, which show a distinct broadening (**Figure *3***). This difference in the strain broadening of reflections which fulfil the non-extinction condition $h+k+l=2n$ (black tick marks in **Figure 3**) and the ones, which do not

(green tick marks in **Figure 3**), was included in the refinement by modification of the peak profile function used by TOPAS with a function $p \cdot \tan(\theta)$ using $p = c$ in the case $h+k+l=2n$ and $p = d$ in the case $h+k+l\neq 2n$. The isotropic displacement parameters of all Ga and Si atoms on the ***6c*** and ***6d*** site were constrained to be equal. Refinement trials with a free Na site occupancy were not successful, thus it was fixed at 0.77(2) with respect to the obtained Si/Ga ratio.

Local environment of silicon: ^{29}Si MAS-NMR – spectroscopy

The ^{29}Si MAS-NMR spectrum of the sample shown in Figure 4 could be fitted using 8 peaks. In the case of a Si/Ga ratio of 1 and space group $P\bar{4}3n$ a single signal could be expected and in the case of a Si/Ga ratio ≠ 1 and space group $I\bar{4}3m$ 5 signals [11]. The result obtained here indicates a ratio M^1/M^2 not equal to one but cannot be attributed to one of the two results given by Gesing [11].

To understand this result, the local environments of Si were evaluated in different structural models. In principle, there are two structural possibilities to be considered:

a) Statistical distribution on the M-site in space group $I\bar{4}3m$ and, as indicated by the experimental results presented so far,
b) A semi-statistical distribution of a certain part of the framework cations in space group $P\bar{4}3n$.

MAS-NMR shows the interaction of an atom with the second nearest neighbour only. Starting with a regular structure in $P\bar{4}3n$, a slice from the a-b plane with 3 layers of metal atoms was taken (in this case all M atoms in the middle layer have four M neighbours) and represented on a matrix, which could be used for distribution simulations analysing the middle layer. The distribution of Ga and Si on the respective sites were calculated according to the two models by varying the distribution coefficients (**Figure *5***). In case a) one overall distribution coefficient was used to distribute Ga and Si on the M site; in case b) the initial distribution is strictly alternating between Si and Ga. Here two distribution coefficients were used to exchange a certain percentage of Ga against Si and vice versa. After this distribution procedure, the neighbourhoods of the Si atoms in the middle layer were analysed, categorized with respect to their Ga amount and displayed in a histogram.

The distribution coefficients were varied, the relative neighbourhood count calculated, collected and compared to the measured spectral intensity distribution.

The Rietveld structure refinement indicates a Si/Ga ratio of 0.89(2) with 14(2)% Si on the Ga site and 17(2)% Ga on the Si site. The modelling of the NMR data shows at first that model b) is correct, it is at all not possible to generate a similar spectral intensity distribution with model a). The best overall agreement between model b) and the observed data (**Figure 6**) was achieved with 13(2)% Si on the Ga site and 10(1)% of Ga on the Si site, leading to a Si/Ga ratio of 0.96(5). Although the qualitative agreement is quite good, the quantitative agreement is of lesser quality. Reasons for this are on one hand the underestimated errors in the site occupancy factors of Si and Ga in the Rietveld refinements and the large uncertainty in the determination of the peak area in the NMR spectrum fitting procedure on the other hand. Nevertheless, the obtained results coincide within one standard deviation (**Figure 6**).

3.2.Thermal dehydration and decomposition

In the TG/DSC measurement only one step in the mass curve with an onset temperature of 603(1) K and an endset temperature of 722(1) K was observed (**Figure *7***). The sample loses 11.2(1)% of its mass which corresponds very well to the calculated 11.5% mass content of 8 H_2O molecules per formula unit. This confirms the interpretation of the FTIR and Raman spectra which excluded the incorporation of OH^- groups into the sodalite cage. The heat flow signal shows a very broad endothermic signal between 587(2) K (onset) and 1118(2) K (endset). It starts at slightly lower temperatures than the mass loss. Within this temperature range it shows several smaller features, two exothermic signals (740 K and 960 K) and an endothermic signal at 860 K. These features could be attributed to a complex bond-breaking process, resulting in the building of six-ring-sheet fragments, which than rearrange themselves at 1118(2) K to form the final beryllonite-type product.

The temperature-dependent X-ray diffraction data were collected between 300 K and 1300 K (**Figure 8**) and the *λ'(10)* parameter of its autocorrelation (**Figure *9***) was determined. The *λ'(10)* parameter is sensible to the number of reflections, their widths and intensities [15], it shows low values around 5 until 600 K, in the temperature range in which the sodalite structure can be observed. The splitting of the reflections at 600 K increases the parameters value to 18. A slightly linear increase to 20 at 860 K indicates the slow and constant loss of scattering intensity. The strong increase in *λ'(10)* and its high maximum at 980 K indicates the complete loss of Bragg scattering intensity (and by this the strong increase of diffuse scattering). The upcoming of a new reflection set (indicating the crystallisation of a new phase) quickly reduces *λ'(10)* to the initial low values at 1000 K.

A similar behaviour was observed by Felsche and Luger [16] in their examinations of the thermal decomposition of different aluminosilicate hydro- and basic/hydro-sodalites in the case of $\left|Na_{6+x}(OH)_x(H_2O)_4\right|[AlSiO_4]_6$. They interpreted this effect as the development of two phases: A fully dehydrated $\left|Na_6\square_2\right|[AlSiO_4]_6$ sodalite on one hand and a $\left|Na_{6+x}(OH)_x\right|[AlSiO_4]_6$ on the other hand. The question arises, if this mechanism is at all possible: If the X-ray diffraction pattern shows only one phase before heating, OH^- and H_2O are statistically distributed over all cages, thus a statistical distribution of empty and OH^- filled cages could be expected after dehydration, resulting in a scattering pattern of one phase with an average lattice parameter. A two-phase system would have been a two-phase system right from the beginning. To get a better insight into the process an indexing of the doubled Bragg reflections was tried. The whole pattern collected at 640 K could be refined by a Pawley-fit in space-group *P*1 and lattice parameters $a = 1261.1(1)$ pm, $b = 1261.3(1)$ pm, $c = 2674.7(1)$ pm, $\alpha = 90.07(1)°$, $\beta = 89.64(1)°$ and $\gamma = 119.38(1)°$. This correspond to a hexagonal setting of the sodalite cell (see **Figure 10**): *a* and *c* of the triclinic cell have

approximately the length of the plane diagonal of the cubic sodalite cage and the triclinic c lattice parameters is approximately three times the sodalites lattice parameter.

This intermediate (INT) phase was included in the batch refinements and its temperature-dependent lattice parameters could be determined. By calculating a pseudo-cubic volume V_{pc} of this phase ($V_{pc} = \frac{a \cdot b}{\sqrt{2}} \cdot \frac{c}{3}$), it was scaled to the size of the initial sodalite (**Figure 11** – left panel). With these cell volumes the thermal expansion coefficients (TEC) were calculated according to $TEC = \frac{1}{V_{Ref}} \cdot \frac{V_n - V_{n-1}}{T_n - T_{n-1}}$ [17] using the lowest temperature at which the phase was observed as the reference temperature (**Figure 11** – right panel). The TEC of the sodalite indicates the beginning dehydration at 500 K by a change of its slope. The strong change in the cell volume between 600 K and 700 K is visible in the TEC by high negative coefficients of the triclinic phase. Between 940 K and 980 K the scattered Bragg intensities of the INT phase vanish completely and the refinement does not give reliable values. The newly upcoming phase at around 1000 K is a hexagonal beryllonite-analogous $NaGa_{1.04}Si_{0.96}O_4$ showing a linear TEC increase until the end of the measurement.

These findings make the following interpretation of the data much more likely: Upon the loss of cage water the sodalite expands with increasing temperature. The strain on the framework (**Figure 12**) is already quite high and increases during the expansion caused by the statistical distribution of Si and Ga on the M sites. This effect is clearly visible in the micro-strain ratio (body-centred forbidden/primitive) of the reflections (**Figure 12** – right panel). The strain of the reflections forbidden by body-centring is 14 times higher than the one of rest of the reflections. The dehydration reduces this ratio, due to an increasing micro-strain of the primitive reflections, by a factor 2. Eventually, this leads to bond breaking of M-O-M bonds in the framework. This process produces fragments of the six-ring sheets with different sizes, visible in the X-ray data by the symmetry reduction to $P1$ and the continuous increase of

diffuse scattering, due to the loss of long range order. The close relation of the proposed triclinic lattice parameters to typical lattice parameters of cancrinites but the much larger *c*-axis parameter indicates a complex stacking (dis)order. The higher the temperature gets the smaller the six-ring sheet fragments become and thus the loss of long range order and Bragg scattering intensity occurs. The sheet fragments can rearrange themselves in a more stable configuration and form a beryllonite type framework with a uniform micro-strain.

4. Summary and conclusion

A new gallosilicate hydro-sodalite was synthesised and its thermal behaviour was studied. Although the Si/Ga ratio deviates from 1 it does not show the expected [11] body-centred structure, but a primitive one with a high micro-strain observable in the reflections which would be symmetry forbidden for the body-centring. This peculiar structure was further examined by spectroscopy techniques: Firstly, vibrational spectroscopy shows pure H_2O without traces of OH^-, confirmed by the TG/DSC measurement. Secondly, the local environment of the Si atoms was examined by ^{29}Si MAS-NMR. The spectrum does neither resemble the published one for the primitive nor the body-centred gallosilicate hydro-sodalite. Different models of Si/Ga distribution were simulated and the resulting spectral intensities calculated: This new technique showed that the model of a primitive structure with occupational disorder on the M^1 and the M^2 sites explains the observed spectrum best. Furthermore, the determined probability coefficients to find Ga on the Si site and vice versa agree very well with the observed respective site occupancy factors.

The temperature-dependent X-ray diffraction data shows some peculiarities as well. After the dehydration of the sodalite a new intermediate phase could be observed, whose scattering intensity vanishes as the temperature increases, and leaves nothing but amorphous scattering contribution before the hexagonal $NaGaSiO_4$ forms. The loss of Bragg-intensity in this

process indicates a complete loss of long-range order, this means a breaking of the framework M-O-M bonds and the formation of $(Ga_{1.04}Si_{0.96}O_4)_3$ sheet fragments. These fragments rearrange and form a stable hexagonal beryllonite type $NaGa_{1.04}Si_{0.96}O_4$ at 1000 K.

5. References

[1] R.X. Fischer, W.H. Baur, *Zeitschrift Für Krist.* **2009**, 224, 185–197.

[2] C. Grader, J. Buhl, *Microporous Mesoporous Mater.* **2013**, 171, 110–117.

[3] K. Hackbarth, M. Fechtelkord, J. Buhl, *React. Kinet. Catal. Lett.* **1998**, 65, 33–39.

[4] G. Hermeler, J. Buhl, W. Hoffmann, *Catal. Today* **1991**, 8, 415–426.

[5] J.C. Buhl, *Thermochim. Acta* **1991**, 178, 19–31.

[6] A. V Borhade, S.G. Wakchaure, *E-Journal Chem.* **2010**, 7, 369–376.

[7] K. Suzuki, Y. Kiyozumi, S. Shin, S. Ueda, *Zeolites* **1985**, 5, 11–14.

[8] L. McCusker, W. Meier, K. Suzuki, S. Shin, *Zeolites* **1986**, 6, 388–391.

[9] J. Newsam, J. Jorgensen, *Zeolites* **1987**, 7, 569–573.

[10] W.T.A. Harrison, T.M. Nenoff, T.E. Gier, G.D. Stucky, *J. Solid State Chem.* **1994**, 113, 168–175.

[11] T. Gesing, *Zeitschrift Für Krist.* **2000**, 215, 510–517.

[12] M.M. Murshed, T.M. Gesing, *Zeitschrift Für Krist.* **2007**, 222, 341–349.

[13] J. Felsche, S. Luger, C. Baerlocher, *Zeolites* **1986**, 6, 367–372.

[14] S. Luger, J. Felsche, P. Fischer, *Acta Crystallogr. Sect. C Cryst. Struct. Commun.* **1987**, 43, 1–3.

[15] L. Robben, *Zeitschrift Für Krist. - Cryst. Mater.* **2017**, 232, 267–277.

[16] J. Felsche, S. Luger, U. Konstanz, *Thermochim. Acta* **1987**, 118, 35–55.

[17] J.D. James, J.A. Spittle, S.G.R. Brown, R.W. Evans, *Meas. Sci. Technol.* **2001**, 12, 1–15.

FIGURES:

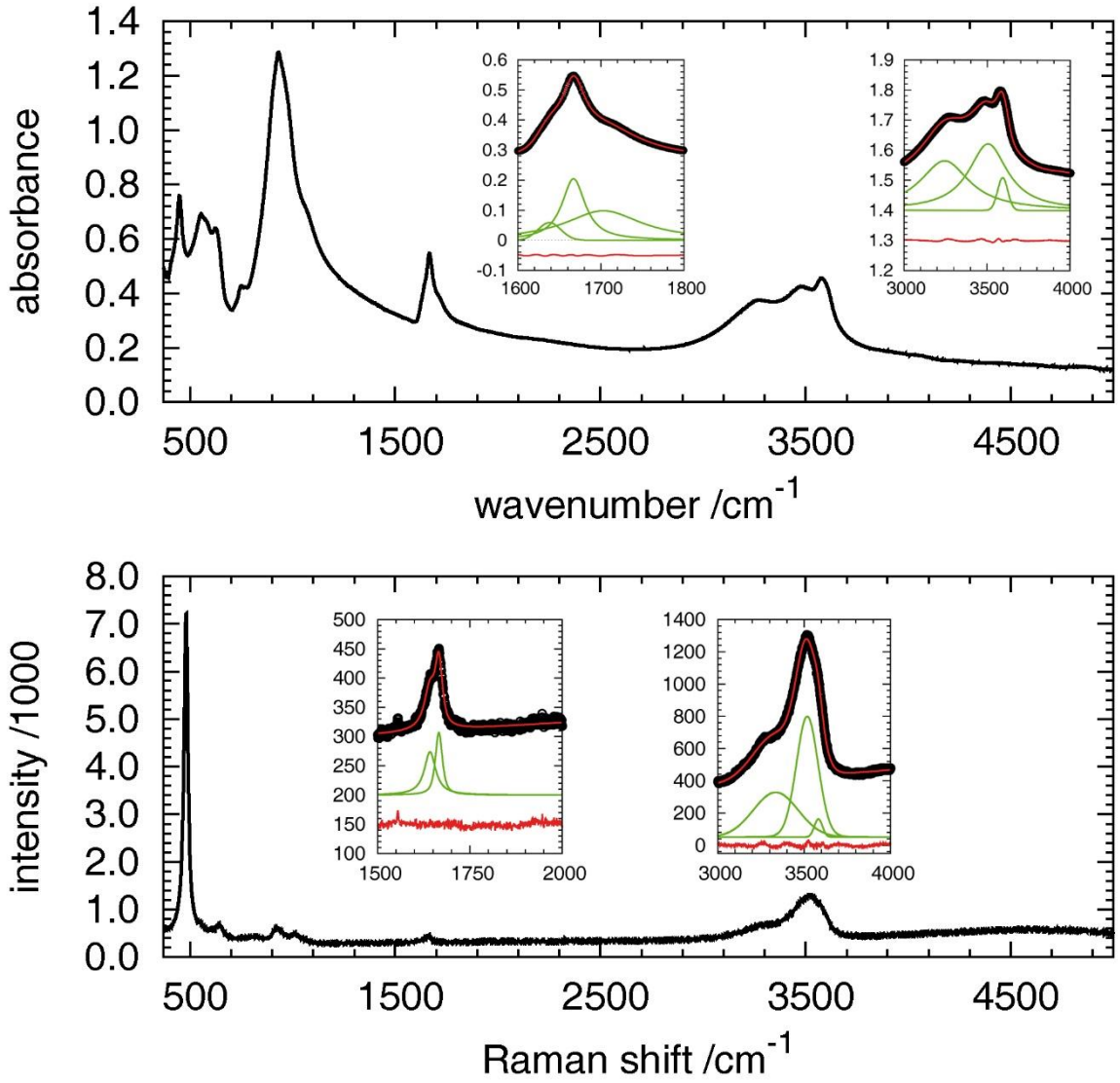

Figure 1: FTIR (top) and Raman (bottom) spectra with peak fitting of the H-O-H bending and the OH-stretching vibrations

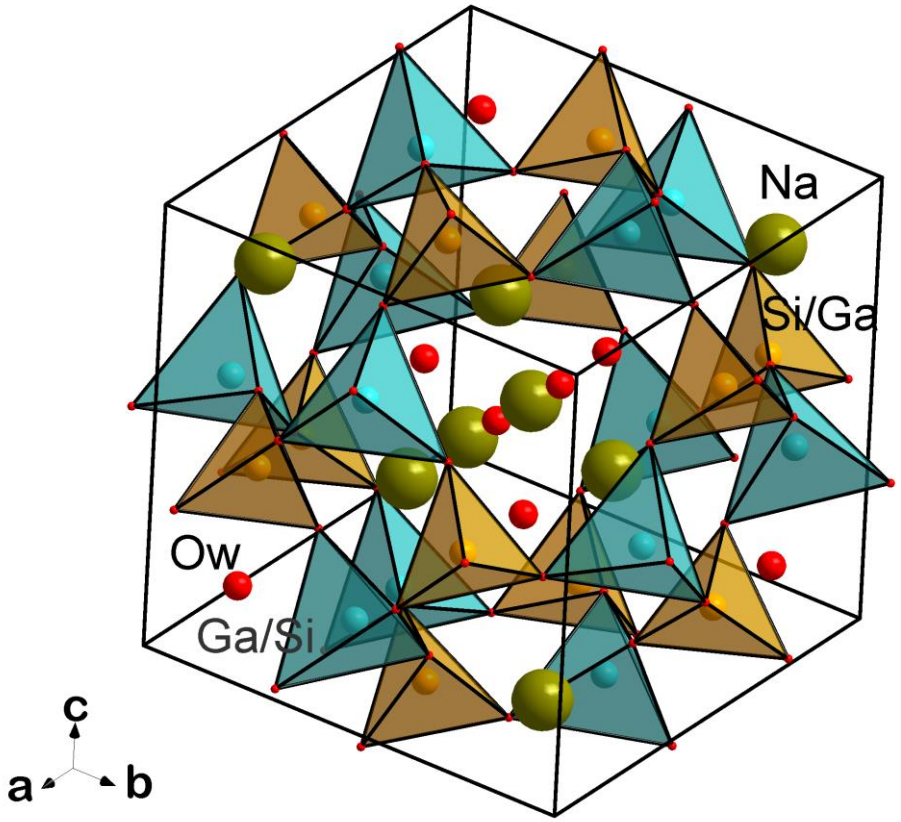

Figure 2: Crystal structure of $\left|Na_{6.16(1)}(H_2O)_8\right|[Ga_{1.04(1)}Si_{0.93(1)}O_4]_6$.

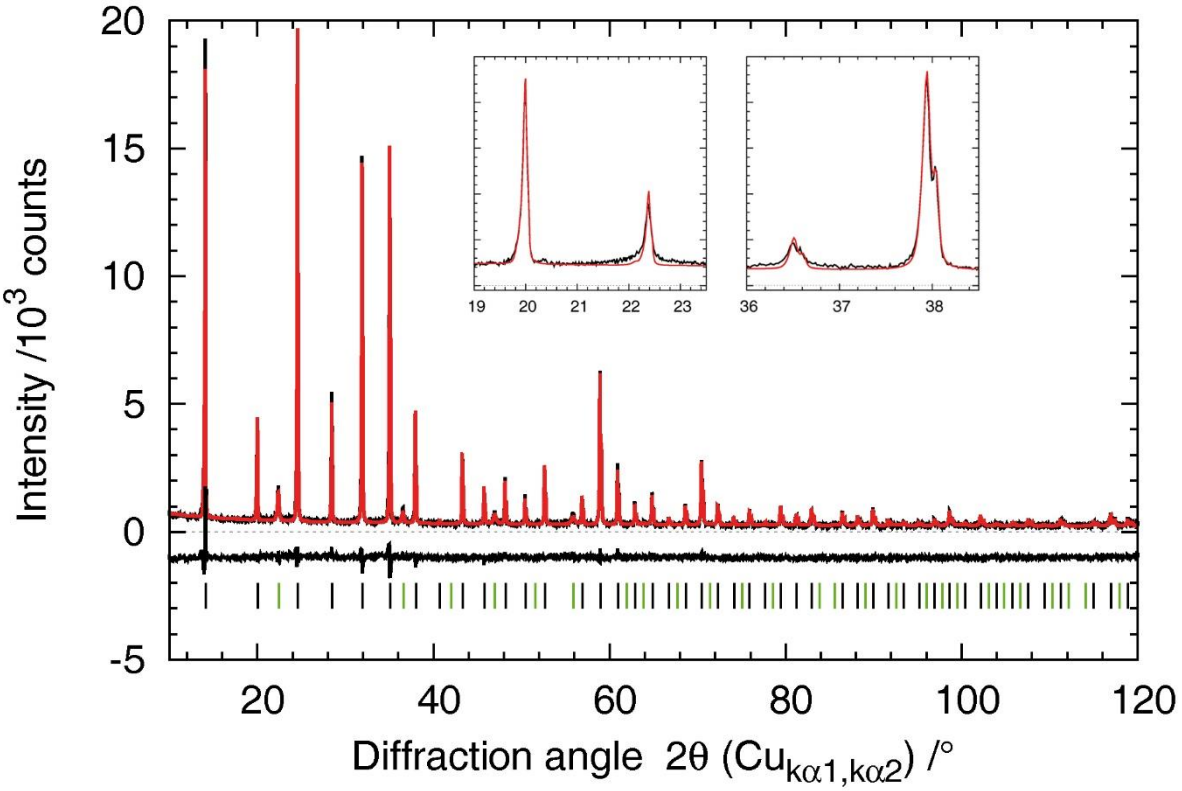

Figure 3: Rietveld-refinement. The insets show the refinement result without considering the anisotropic peak broadening for two selected reflections. Green reflection markers indicate reflections forbidden by symmetry in the body-centered space group.

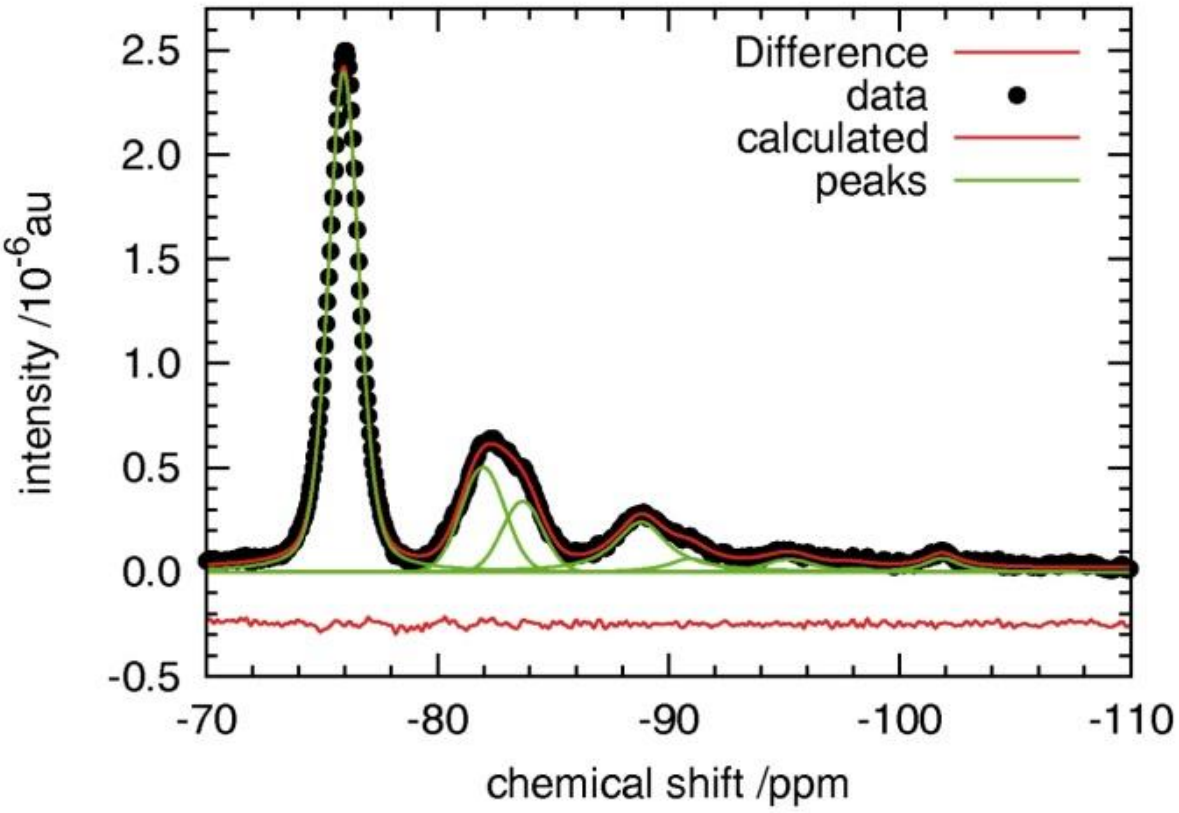

Figure 4: ^{29}Si MAS-NMR spectrum with 8 peaks fitting

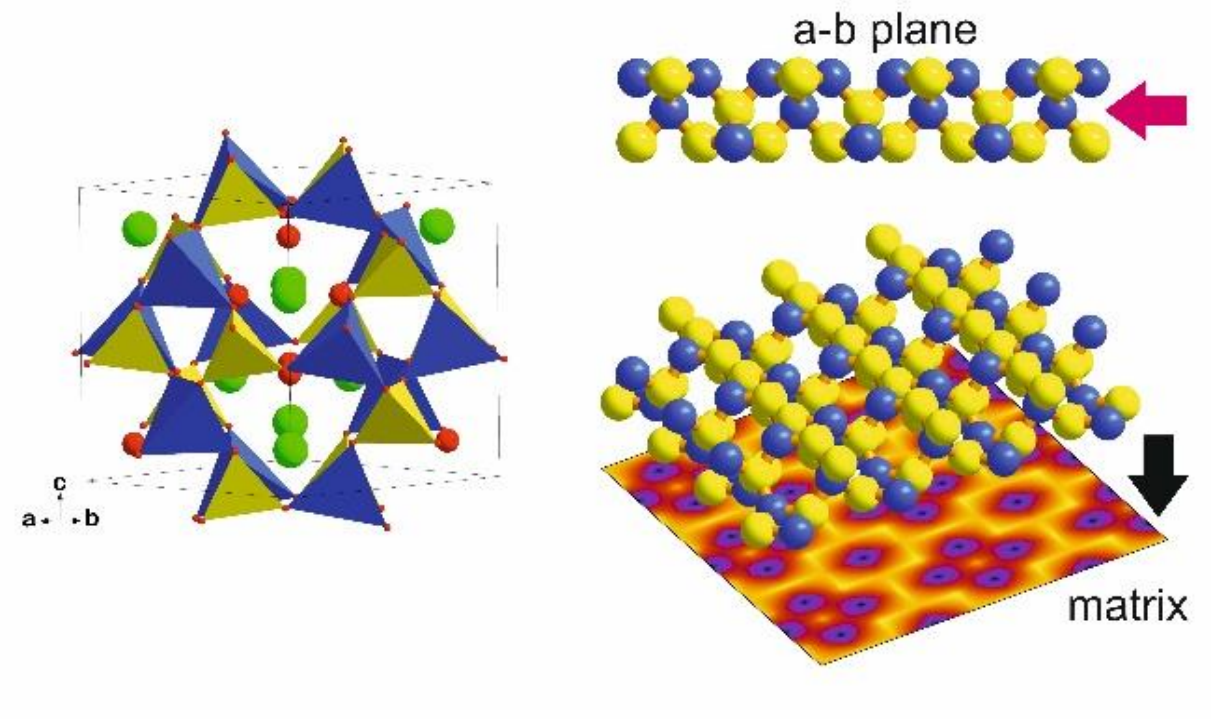

Figure 5: Scheme to visualize the principle of the modelling of local Si environments. A slice containing three layers of M atoms was cut from the a-b plane. The cut was projected on a two-dimensional matrix and Ga and Si atoms were attributed to the sites according to the models described in the text.

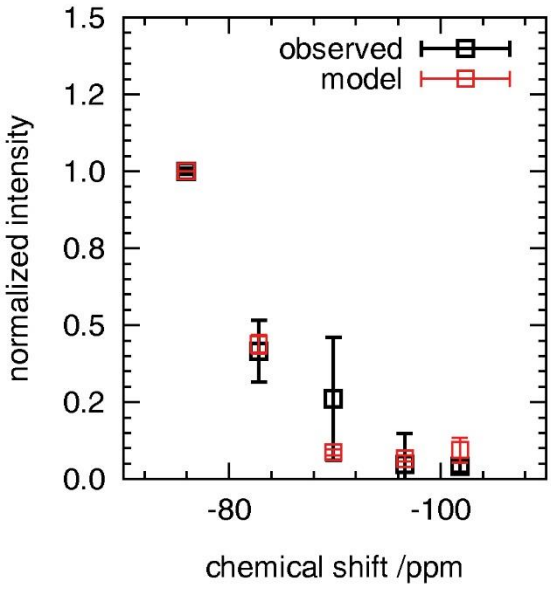

Figure 6: Observed integrated areas of the NMR spectra peaks (black – normalized to the highest value) and the relative number of neighbourhoods from the modelling (red) for the best fitting model.

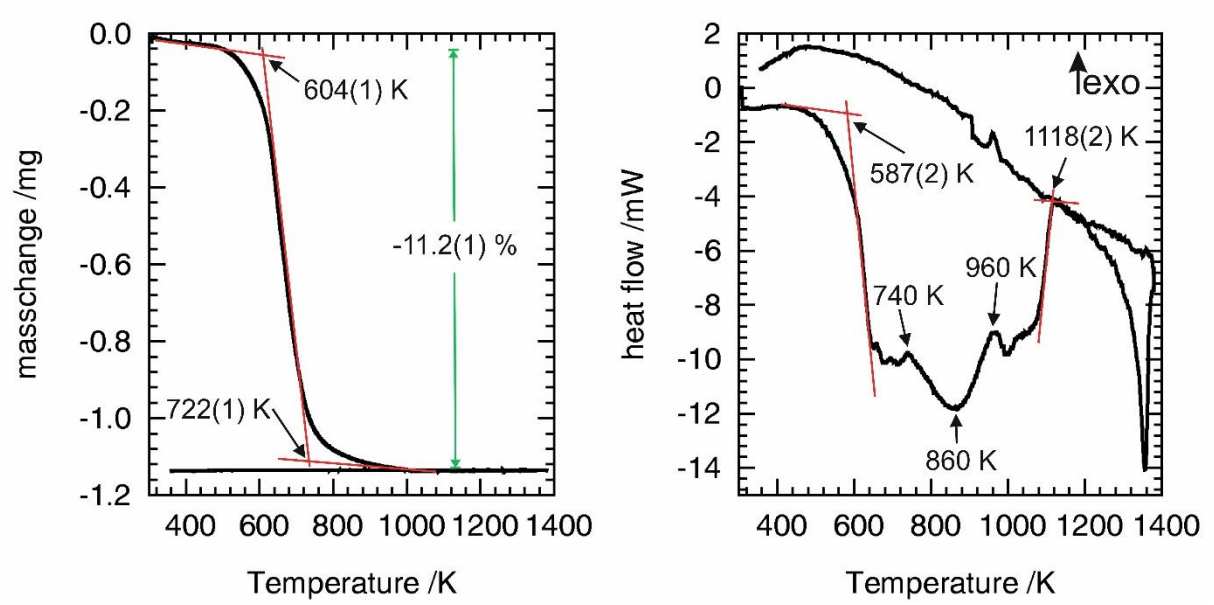

Figure 7: TG/DTA measurement (mass curve: left panel; heat flow: right panel; sample mass: 9.962(1) mg)

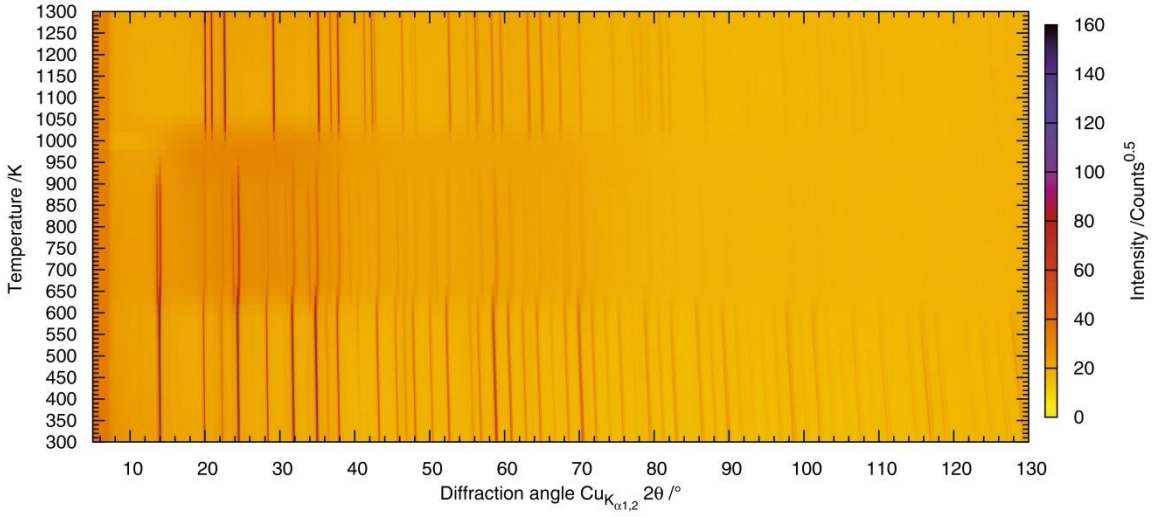

Figure 8: Temperature-dependent X-ray diffraction pattern of $|Na_6(H_2O)_8|[Ga_{1.04(1)}Si_{0.96(1)}O_4]_6$

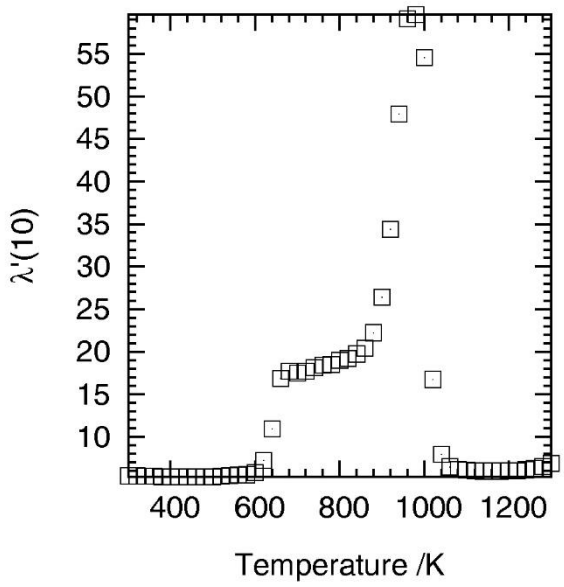

Figure 9: The *λ'(10)* parameter from the autocorrelation of the temperature-dependent X-ray diffraction pattern.

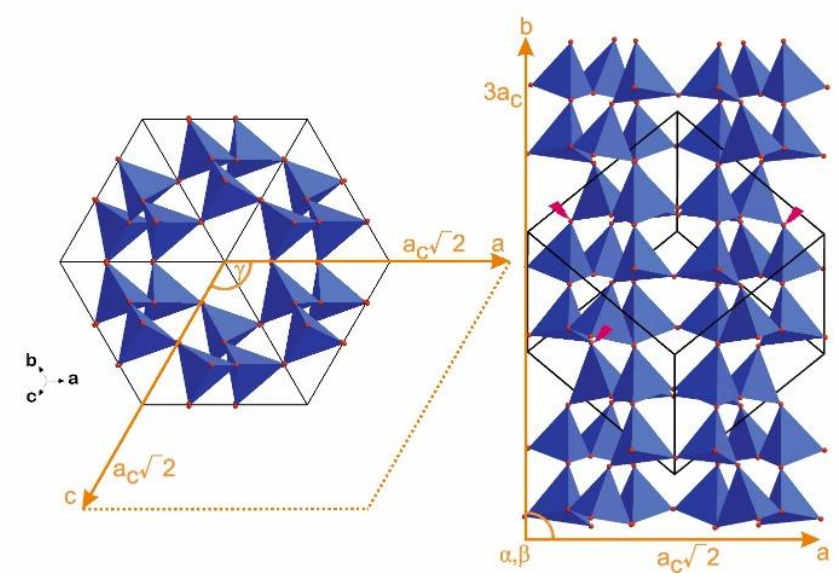

Figure 10: Structural relationship between the sodalite structure and the triclinic cell used in the Pawley-fits after the sodalites dehydration (red symbols indicate some breaking points for the sheet formation).

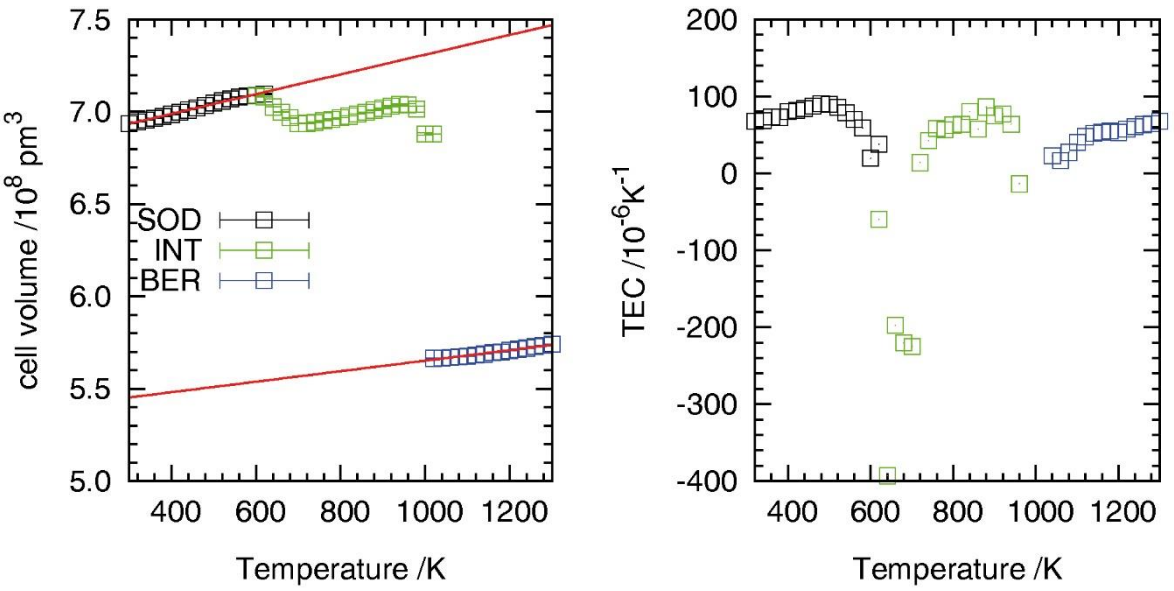

Figure 11: Temperature-dependent cell volume (left) and thermal expansion coefficients TEC (right).

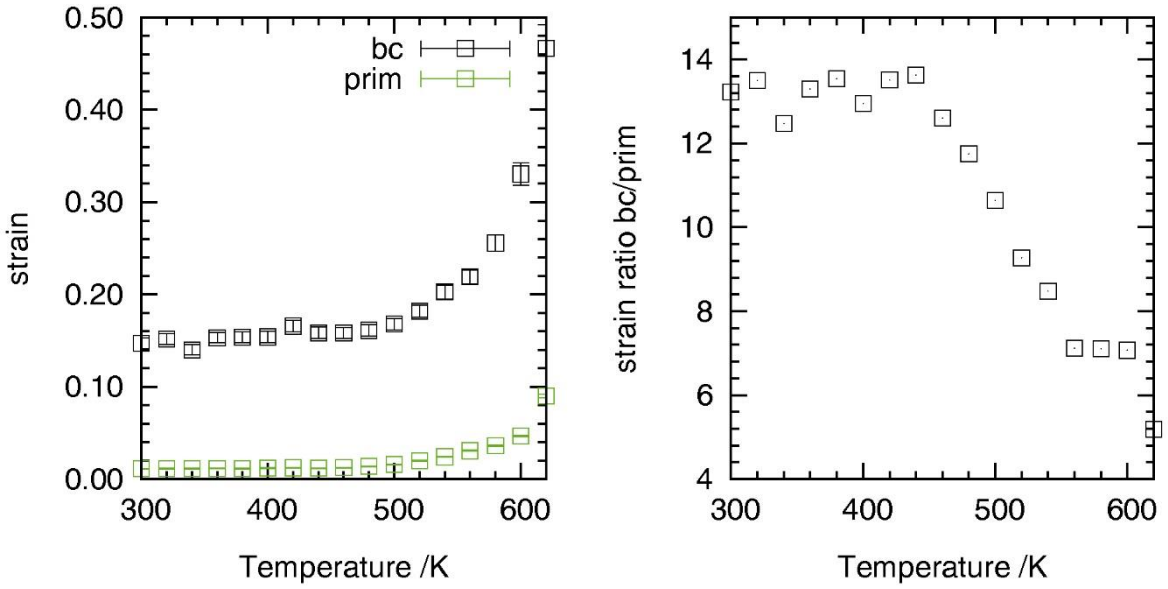

Figure 12: Micro-strain of the body-centered forbidden (bc) and all others (prim) reflections (left panel). Their ratio (bc/prim - right panel) indicates the start of the dehydration by a strong decrease.

TABLES:

Table 1: Details of PXRD data collection and refinement of $|Na_{6.16(1)}(H_2O)_8|[Ga_{1.04(1)}Si_{0.93(1)}O_4]_6$

Powder	white, <63 µm
Wavelength /pm	154.0596(1), 154.4493(1)
μ /cm^{-1}	113.2(5)
$2\theta_{min}$ /°	10
$2\theta_{max}$ /°	130
2θ *stepwidth*	0.0167
$N(points)_{measured}$	7480
$N(hkl)_{measured}$	125
$N(parameter)_{refined}$	21
space group	$P\bar{4}3n$
a /pm	885.374(5)
Volume /10^6 pm^3	693.65(2)
T /K	300(1)
R_{wp}	8.74
R_{Bragg}	2.21

Table 2: Atomic parameters of $\left|Na_{6.16(1)}(H_2O)_8\right|[Ga_{1.04(1)}Si_{0.93(1)}O_4]_6$ (equal values are constrained to each other)

Atom	*Site*	*x*	*y*	*z*	*occupancy*	B_{iso}
Ga1	6d	1/4	0	1/2	0.17(1)[#]	0.73(2)[a]
Si1					0.83(1) [#]	0.73(2)[a]
Si2	6c	1/4	1/2	0	0.14(2) [#]	0.73(2)[a]
Ga2					0.86(2) [#]	0.73(2)[a]
O1	24i	0.1503(3)	0.1331(3)	0.4246(3)	1	1.0(1)
Na1	8e	0.14324)	x	x	0.77(2)	3.6(2)
Ow	8e	0.37285(38)	x	x	1	3.1(3)

[#] constrained to unity on each site, [a]constrained to each other